Available online at www.sciencedirect.com
SCIENCE DIRECT®
Comput. Methods Appl. Mech. Engrg. 193 (2004) 2019–2032
Computer methods in applied mechanics and engineering
www.elsevier.com/locate/cma

Automatic mesh update with the solid-extension mesh moving technique

Keith Stein [a,*], Tayfun E. Tezduyar [b], Richard Benney [c]

[a] Department of Physics, Bethel College, St. Paul, MN 55112, USA
[b] Mechanical Engineering, Rice University—MS 321, 6100 Main Street, Houston, Texas 77005, USA
[c] US Army Natick Soldier Center, Kansas Street, Natick, MA 01760, USA

Received 13 February 2003; received in revised form 15 July 2003; accepted 8 December 2003

Abstract

In computation of fluid–structure interactions involving large displacements, we use a mesh update method composed of mesh moving and remeshing-as-needed. For problems with complex geometries, we need automatic mesh moving techniques that reduce the need for remeshing. We also would like that these mesh moving techniques allow us to control mesh resolution near the fluid–structure interfaces so that we can represent the boundary layers more accurately. In the mesh moving techniques we designed, the motion of the nodes is governed by the equations of elasticity, and mesh deformation is handled selectively based on element sizes and deformation modes. This is helping us reduce the frequency of remeshing. With the solid-extension mesh moving technique presented in this paper, we are also able to limit mesh distortion in thin layers of elements placed near fluid–structure interfaces.

Keywords: Mesh moving; Fluid–structure interactions; Solid-extension mesh moving technique

1. Introduction

Interface-tracking methods are well-suited for problems where precise representation of moving interfaces is needed in the fluid mesh. In these methods, the mesh is updated and the spatial domain of the fluid deforms to track the motion of the interface in time. In the computation of fluid–structure interactions, we use our mesh update techniques with the deforming-spatial-domain/stabilized space–time (DSD/SST) formulation [1–3], which is an interface-tracking technique. The DSD/SST formulation was developed for computation of flows with moving boundaries and interfaces, including fluid–structure interactions. While the DSD/SST formulation is our method of choice, it should be noted that our mesh update techniques could also be used with the arbitrary Lagrangian–Eulerian method, another interface-tracking method.

* Corresponding author. Tel.: +1-651-638-6173; fax: +1-651-638-6001.
E-mail addresses: k-stein@bethel.edu (K. Stein), tezduyar@rice.edu (T.E. Tezduyar), richard.benney@natick.army.mil (R. Benney).

0045-7825/$ - see front matter
doi:10.1016/j.cma.2003.12.046

Remeshing is computationally burdensome for 3D computations with complex geometries. This process typically involves calling an automatic (unstructured) mesh generator and projecting the solution from the old mesh to the new one. In addition to the computational burden, the remeshing step introduces projection errors into the numerical solution. Both of these issues motivate us to develop a mesh update method consisting of moving the mesh as long as possible, and full or partial remeshing when element distortion becomes excessive. In mesh moving, the normal velocity for the mesh and fluid must match at the interface. Upon satisfying this condition, our goal in designing the mesh update technique becomes reducing the frequency of remeshing. This can be achieved by controlling mesh distortion for the overall mesh, but also specifically for the layers of elements next to the interface, where the consequences of mesh distortion are most severe.

In most real-world applications, such as parachute fluid–structure interactions, problem geometries are complex and require automatic methods for mesh generation and mesh update. We use an automatic mesh moving technique, introduced in [4], where motion of mesh nodes is governed by the equations of elasticity, and the mesh deformation is handled selectively based on the element sizes and deformation modes. Deformation modes are described in terms of shape and volume changes. As boundary condition, motion of the interface nodes is required to match the normal velocities of the fluid. With the boundary condition satisfied, motion of the internal nodes is determined by solving the equations of elasticity. Mesh moving techniques with comparable features were introduced in [5].

Various approaches for selective treatment of the mesh deformation have been taken to improve mesh moving behavior. In [4], selective treatment based on shape and volume changes is attained by adjusting the relative values of the Lamé constants of the elasticity equations. Here, the interest is to stiffen the mesh against shape changes more than against volume changes. Selective treatment based on element sizes, on the other hand, is attained by altering the way the Jacobian of the transformation from the element domain to the physical domain is accounted for. In this case, the objective is to increase stiffening of the smaller elements, which are typically located near solid surfaces and, without selective treatment, can absorb excessive amounts of the mesh deformation. A more extensive type of this Jacobian-based stiffening was presented in [6] by introducing a stiffening power that determines the degree by which the smaller elements are rendered stiffer than the larger ones. In this context, by varying the stiffening power, a family of mesh moving techniques is generated.

In some problems, structured layers of elements are needed to fully control mesh resolution around solid objects and boundaries and to more accurately represent boundary layers. For non-deforming solid objects (i.e. rigid bodies), the user has full control of the mesh resolution in the layers and the structured layers can move ''glued'' to the solid body as it undergoes rigid-body motion as demonstrated in [4].

Here, no equations are solved for the motion of the nodes in these layers, because these nodal motions are not governed by the equations of elasticity. This results in some cost reduction. For early examples of automatic mesh moving combined with structured layers of elements undergoing rigid-body motion with solid objects, see [7]. Earlier examples of element layers undergoing rigid-body motion, in combination with deforming structured meshes, can be found in [1].

In computation of flows with fluid–solid interfaces where the solid is deforming, limiting mesh distortion in the very thin fluid elements near the solid surface becomes a necessary and challenging objective for automatic mesh moving techniques. In these cases, the motion of the fluid mesh near the interface cannot be represented by a rigid-body motion. The solid-extension mesh moving technique (SEMMT), introduced in [8,9], treats the very thin fluid elements much like an extension of the solid elements. In the SEMMT, motion of the fluid nodes is governed by the equations of elasticity, but special treatment of the elements in thin layers results in reduced distortion of those elements. Two ways of accomplishing this were proposed in [8,9]; solving the elasticity equations for the nodes connected to the thin (inner) elements separate from the elasticity equations for the other nodes, or together. If we solve them separately, for the inner elements, as boundary conditions at the interface with the other elements, we would use traction-free conditions. In [10]

the separate solution option was referred to as "SEMMT—multiple domain" (SEMMT-MD) and the unified solution option as "SEMMT—single domain" (SEMMT-SD). Early reports from test computations for translation, rotation, and bending tests were also included in [10].

In the following sections we describe our mesh moving technique and demonstrate its performance for several 2D test cases. In Section 2, we first present the governing equations of linear elasticity and the corresponding finite element formulation. Then we describe how the SEMMT can be used to treat selectively the thin layers of elements. In Section 3 we present results from a set of 2D mesh deformation test cases. In Section 4 we show how the SEMMT works for a simple, 2D fluid–structure interaction model problem. Concluding remarks are given in Section 5.

2. Solid-extension mesh moving technique

The SEMMT is based on treating the very thin fluid elements much like an extension of the solid elements. In the following subsections we describe the specific components of the SEMMT.

2.1. Equations of linear elasticity

Let $\Omega \subset \mathbb{R}^{n_{\text{sd}}}$ be the spatial domain bounded by Γ, where n_{sd} is the number of space dimensions. Corresponding to the Dirichlet- and Neumann-type boundary conditions, the boundary Γ is composed of Γ_g and Γ_h. The equations governing the displacement of the internal nodes can then be written as

$$\nabla \cdot \boldsymbol{\sigma} + \mathbf{f} = \mathbf{0} \quad \text{on } \Omega, \tag{1}$$

where $\boldsymbol{\sigma}$ is the Cauchy stress tensor and $\mathbf{f}$ is the external force. For linear elasticity, $\boldsymbol{\sigma}$ is defined as

$$\boldsymbol{\sigma} = \lambda \operatorname{tr}(\boldsymbol{\varepsilon}(\mathbf{y}))\mathbf{I} + 2\mu\boldsymbol{\varepsilon}(\mathbf{y}), \tag{2}$$

where $\mathbf{y}$ is the displacement, tr( ) is the trace operator, λ and μ are the Lamé constants, $\mathbf{I}$ is the identity tensor, and $\boldsymbol{\varepsilon}(\mathbf{y})$ is the strain tensor:

$$\boldsymbol{\varepsilon}(\mathbf{y}) = \tfrac{1}{2}(\nabla\mathbf{y} + (\nabla\mathbf{y})^{\mathbf{T}}). \tag{3}$$

The Dirichlet- and Neumann-type boundary conditions are represented as

$$\mathbf{y} = \mathbf{g} \quad \text{on } \Gamma_g, \qquad \mathbf{n} \cdot \boldsymbol{\sigma} = \mathbf{h} \quad \text{on } \Gamma_h. \tag{4}$$

2.2. Finite element formulation

In writing the finite element formulation for Eq. (1), we first define the finite element trial and test function spaces $\mathscr{S}^h$ and $\mathscr{V}^h$:

$$\mathscr{S}^h = \{\mathbf{y}^h \mid \mathbf{y}^h \in [H^{1h}(\Omega)]^{n_{\text{sd}}}, \mathbf{y}^h \doteq \mathbf{g}^h \text{ on } \Gamma_g\}, \tag{5}$$

$$\mathscr{V}^h = \{\mathbf{w}^h \mid \mathbf{w}^h \in [H^{1h}(\Omega)]^{n_{\text{sd}}}, \mathbf{w}^h \doteq \mathbf{0} \text{ on } \Gamma_g\}. \tag{6}$$

Here, $H^{1h}(\Omega)$ is the finite-dimensional function space over Ω. This space is formed over the element domain using continuous first-order polynomials in space. The finite element formulation for Eq. (1) is then written as follows: find $\mathbf{y}^h \in \mathscr{S}^h$ such that $\forall \mathbf{w}^h \in \mathscr{V}^h$

$$\int_\Omega \boldsymbol{\varepsilon}(\mathbf{w}^h) : \boldsymbol{\sigma}(\mathbf{y}^h)\, \mathrm{d}\Omega - \int_\Omega \mathbf{w}^h \cdot \mathbf{f}\, \mathrm{d}\Omega = \int_{\Gamma_h} \mathbf{w}^h \cdot \mathbf{h}\, \mathrm{d}\Gamma. \tag{7}$$

In our examples, no external forcing function is defined to selectively handle mesh motion, so the force vector $\mathbf{f}$ is set to zero.

2.3. Jacohian-based stiffening

Mesh deformation is selectively treated by altering the way we account for the Jacobian of the transformation from the element domain to the physical domain. This method was first introduced in [4], where the Jacobian is dropped from the finite element formulation, resulting in the smaller elements being stiffened more than the larger ones. The method described in [4] was augmented in [6] to a more extensive kind by introducing a stiffening power that determines the degree by which the smaller elements are rendered stiffer than the larger ones. To describe the method, we first write the global integrals generated by the terms in Eq. (7) as

$$\int_{\Omega} [\cdots] \, \mathrm{d}\Omega = \sum_{e} \int_{\Xi} [\cdots]^{e} J^{e} \, \mathrm{d}\Xi, \tag{8}$$

where $[\cdots]$ symbolically represents what is being integrated, Ξ is the finite element (parent) domain, and the Jacobian for element e is defined as $J^{e} = \det(\partial \mathbf{x}/\partial \boldsymbol{\xi})^{e}$, with $\mathbf{x}$ and $\boldsymbol{\xi}$ representing the physical and element (local) coordinates.

We alter the way we account for the Jacobian as follows:

$$\int_{\Xi} [\cdots]^{e} J^{e} \, \mathrm{d}\Xi \mapsto \int_{\Xi} [\cdots]^{e} J^{e} \left(\frac{J^{0}}{J^{e}} \right)^{\chi} \mathrm{d}\Xi, \tag{9}$$

where χ, a non-negative number, is the stiffening power, and J^{0}, an arbitrary scaling parameter, is inserted into the formulation to make the alteration dimensionally consistent. With $\chi = 0.0$, the method reduces back to an elasticity model with no Jacobian-based stiffening. With $\chi = 1.0$, the method is identical to the one first introduced in [4]. In the general case of $\chi \neq 1.0$, the method stiffens each element by a factor of $(J^{e})^{-\chi}$, and χ determines the degree by which the smaller elements are rendered stiffer than the larger ones.

2.4. Options for SEMMT: SEMMT-MD and SEMMT-SD

In the SEMMT-MD option, we solve the elasticity equations for the nodes connected to the thin (inner) elements separately from the elasticity equations for the other nodes. As boundary conditions at the interface with the other elements, we use traction-free conditions. In the SEMMT-SD option, we solve the elasticity equations for all the nodes together, but stiffen the inner elements to a greater extent. This is accomplished in the following examples by setting $\chi = 2.0$ for those elements while leaving it at the standard value of $\chi = 1.0$ for the outer elements.

3. Mesh deformation test cases

We present mesh deformation test cases for a 2D unstructured mesh consisting of triangular elements and an embedded structure with zero thickness. The mesh spans a region of $|x| \leqslant 1.0$ and $|y| \leqslant 1.0$. The structure spans $y = 0.0$ and $|x| \leqslant 0.5$. Three layers of elements (with $\ell_y = 0.01$) are placed along each side of the structure, with 50 element edges along the structure (i.e. $\ell_x = 0.02$). Fig. 1 shows the mesh and its close-up view near the structure.

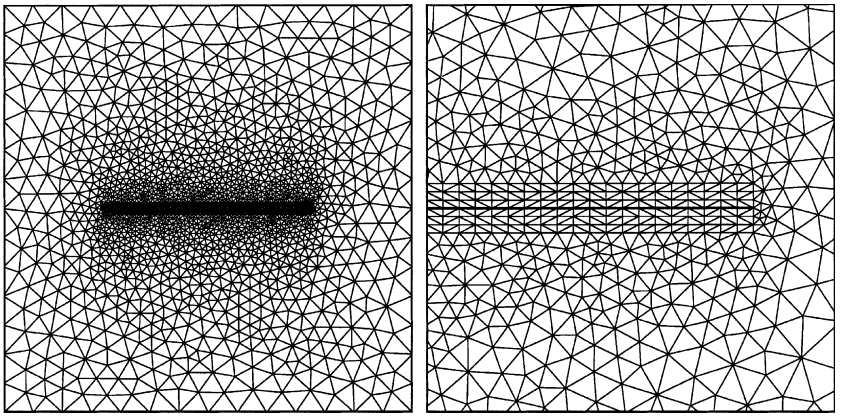

Fig. 1. 2D test mesh for SEMMT.

3.1. General test conditions and mesh quality measures

The test cases involve three different types of prescribed motion or deformation for the structure identical to the motions prescribed in [6]: rigid-body translation in the y-direction, rigid-body rotation about the origin, and prescribed bending. In the case of prescribed bending, the structure deforms from a line to a circular arc, with no stretch in the structure and no net vertical or horizontal displacement. For each test case the maximum displacement or deformation is reached over 50 increments. Those maximum values are $\Delta y = 0.5$ for the translation test, a rotation of $\Delta\theta = \pi/4$ for the rotation test, and bending to a half-circle ($\theta = \pi$) for the bending test.

The mesh over which the elasticity equations are solved is updated at each increment. This update is based on the displacements calculated over the current mesh that has been selectively stiffened. That way, the element Jacobians used in stiffening are updated every time the mesh deforms. As a result, the most current size of an element is used in determining how much it is stiffened. Also as a result, as an element approaches a tangled state, its Jacobian approaches zero, and its stiffening becomes very large.

To evaluate the effectiveness of different mesh moving techniques, two measures of mesh quality are defined, similar to those in [11]. They are *element-area change* ($\mathrm{f}^e_{\mathrm{A}}$) and *element shape change* ($\mathrm{f}^e_{\mathrm{AR}}$):

$$\mathrm{f}^e_{\mathrm{A}} = \left|\log\left(\frac{A^e}{A^e_o}\right)\right|, \qquad \mathrm{f}^e_{\mathrm{AR}} = \left|\log\left(\frac{\mathrm{AR}^e}{\mathrm{AR}^e_o}\right)\right|. \tag{10}$$

Here subscript "o" refers to the undeformed mesh (i.e. the mesh obtained after the last remesh) and AR^e is the element aspect ratio, defined as

$$\mathrm{AR}^e = \frac{(\ell^e_{\max})^2}{A^e}, \tag{11}$$

where $\ell^e_{\max}$ is the maximum edge length for element e.

We define array norms for the set of element mesh quality measures as

$$\|\mathsf{f}_{\mathrm{A}}\|_p = \left\{\sum_e (\mathrm{f}^e_{\mathrm{A}})^p\right\}^{1/p}, \qquad \|\mathsf{f}_{\mathrm{AR}}\|_p = \left\{\sum_e (\mathrm{f}^e_{\mathrm{AR}})^p\right\}^{1/p}, \tag{12}$$

where f_{A} and f_{AR} are the arrays of mesh quality values f_{A} and f_{AR} for all elements of interest, and p is the norm of interest. In the following examples, we will consider the norm where $p = \infty$, and

$$\|\mathbf{f}_{\mathrm{A}}\|_{\infty} = \max_{e} (\mathrm{f}^{e}_{\mathrm{A}}), \qquad \|\mathbf{f}_{\mathrm{AR}}\|_{\infty} = \max_{e} (\mathrm{f}^{e}_{\mathrm{AR}}). \tag{13}$$

Thus, for a given set of mesh elements, global area and shape changes are defined to be the maximum values of the element-area and shape changes, respectively.

3.2. Test results

The tests are carried out with the standard technique (where $\chi = 1.0$ for all the elements and all the nodes are moved together), SEMMT-SD (with $\chi = 2.0$ for the inner elements and $\chi = 1.0$ for the outer elements), and SEMMT-MD (with $\chi = 1.0$ for all elements in both domains).

Fig. 2 shows, for SEMMT-MD, the deformed mesh for the translation, rotation, and bending tests. Fig. 3 shows, in close-up views, comparison of these meshes with the deformed meshes obtained with the standard technique and the SEMMT-SD approach. In this figure, inner elements are colored to indicate the

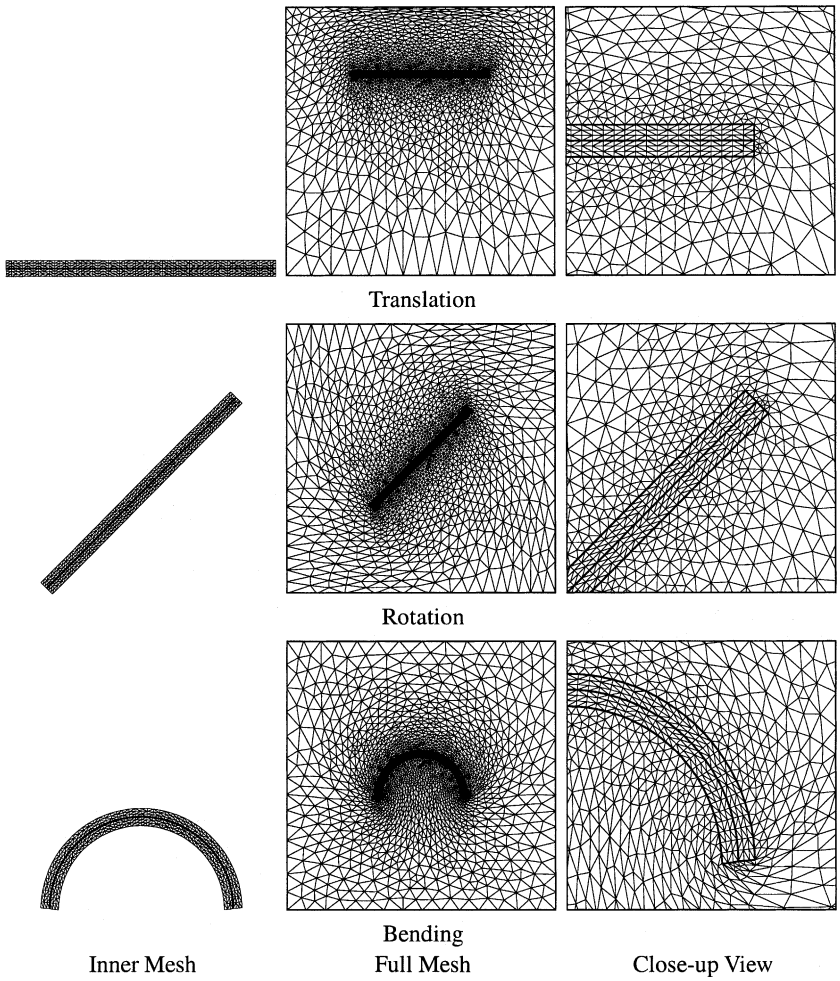

Fig. 2. Mesh deformation tests with SEMMT-MD.

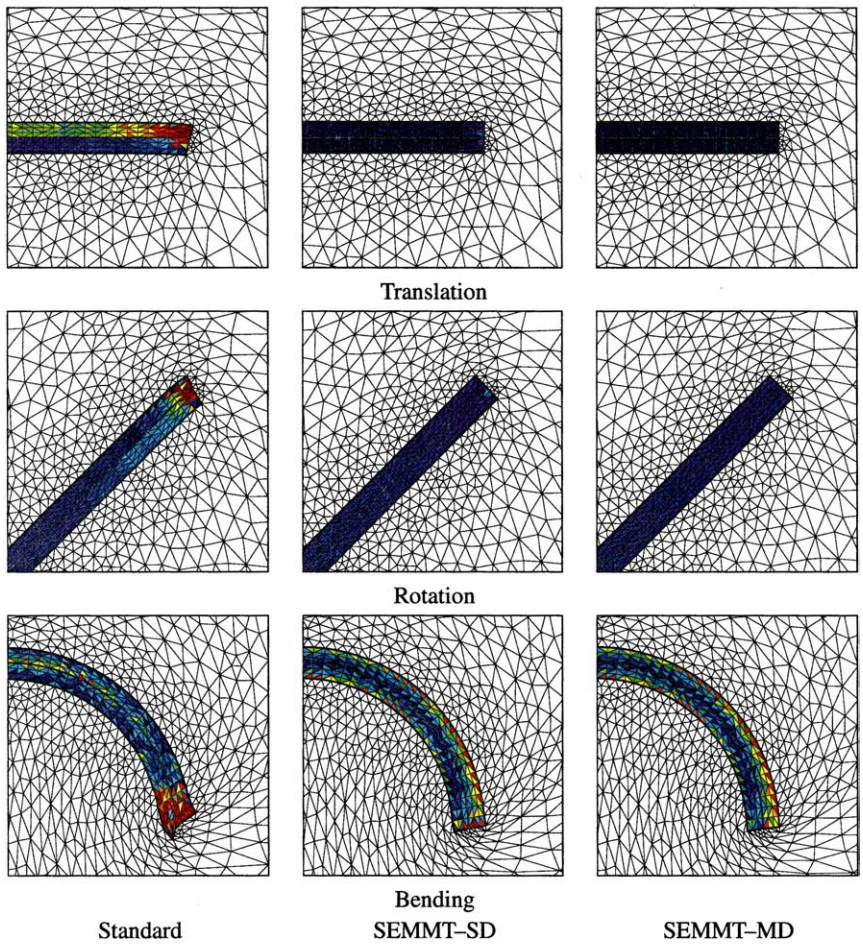

Fig. 3. Mesh deformation tests with the standard mesh moving technique, SEMMT-SD, and SEMMT-MD.

level of element-area distortion, with blue and red corresponding to low and high distortion, respectively. It is evident from the figure that the standard technique allows for significant distortion of the inner elements, particularly for the bending motion. It is also clear that the SEMMT approach reduces distortion in the inner elements.

Fig. 4 shows, for the bending test, the two mesh quality measures (defined based on all the elements) for the standard technique, SEMMT-SD, and SEMMT-MD. The curves show the mesh quality as a function of the bending magnitude, and indicate an improvement in overall mesh quality for the SEMMT over the standard technique. Improvements of 30–50% are seen for elemental area distortion, while smaller improvements are seen for elemental aspect ratio distortion. Performance for the two SEMMT approaches are very comparable.

As stated earlier, the strength of the SEMMT method lies in the handling of mesh motion in thin layers of elements. When we compare performance of the SEMMT with the standard technique for the inner elements (i.e. layers) we see a more dramatic improvement than we do for the overall mesh motion. Fig. 5 shows, for the translation test, the two mesh quality measures (defined based on the inner elements) plotted as functions of the translation magnitude for the standard technique, SEMMT-SD, and SEMMT-MD. The

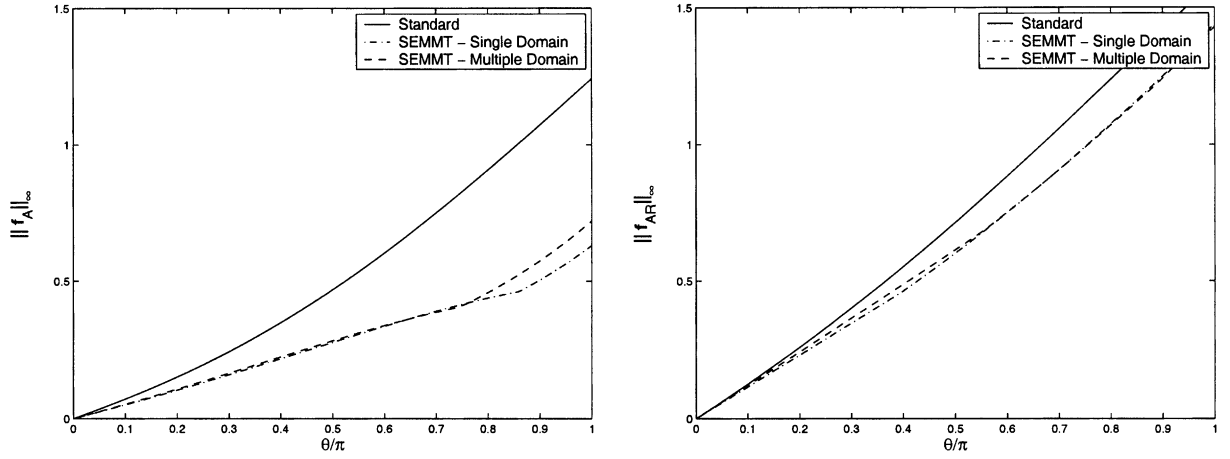

Fig. 4. Bending test mesh quality (defined based on all the elements) as function of bending magnitude, for the standard mesh moving technique, SEMMT-SD, and SEMMT-MD.

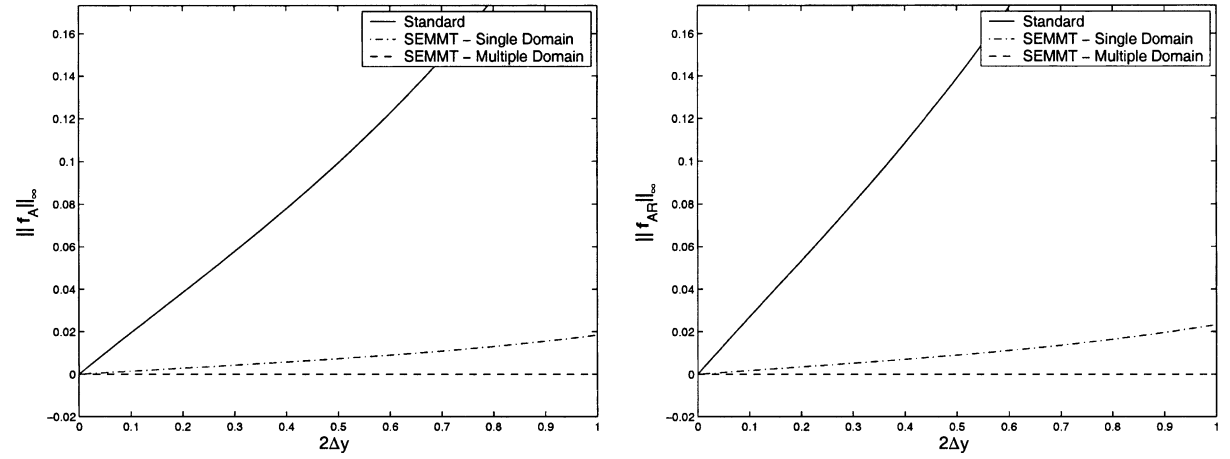

Fig. 5. Translation test mesh quality (defined based on the inner elements) as function of translation magnitude, for the standard mesh moving technique, SEMMT-SD, and SEMMT-MD.

SEMMT approach yields significant reductions over the mesh distortion encountered with the standard technique. Reductions in distortion over the standard technique of approximately 92% are experienced for the SEMMT-SD approach. For rigid-body translation, zero distortion is introduced to the inner mesh for the SEMMT-MD approach. For the mesh quality measures defined based on all the elements, there is little difference between the three mesh moving techniques.

Fig. 6 shows, for the rotation test, the two mesh quality measures (defined based on the inner elements) plotted as functions of the rotation magnitude for the standard technique, SEMMT-SD, and SEMMT-MD. Reductions in distortion over the standard technique of approximately 91–92% are experienced for the SEMMT-SD approach. The reductions are approximately 95–98% for the SEMMT-MD approach. For the mesh quality measures defined based on all the elements, there is little difference between the three mesh moving techniques.

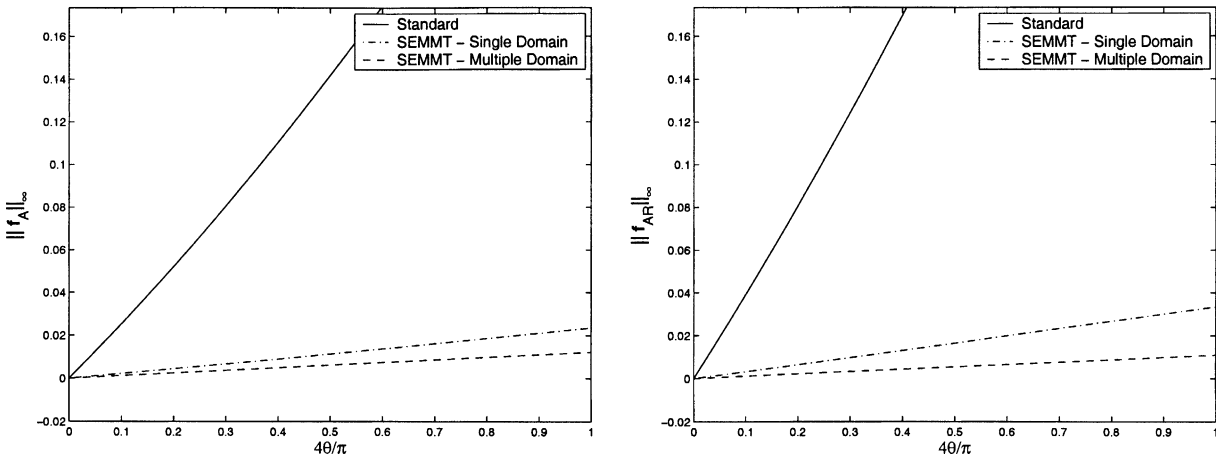

Fig. 6. Rotation test mesh quality (defined based on the inner elements) as function of rotation magnitude, for the standard mesh moving technique, SEMMT-SD, and SEMMT-MD.

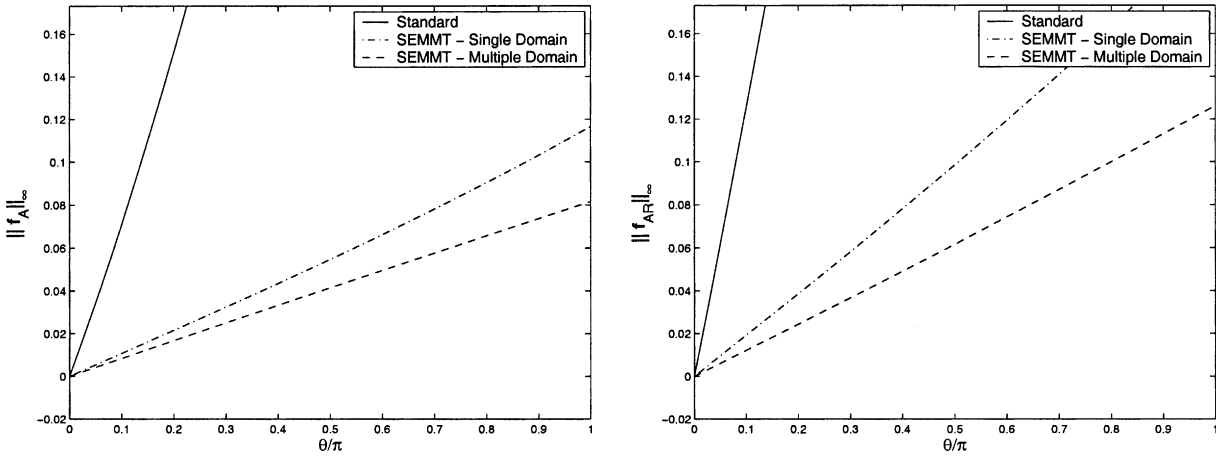

Fig. 7. Bending test mesh quality (defined based on the inner elements) as function of bending magnitude, for the standard mesh moving technique, SEMMT-SD, and SEMMT-MD.

Fig. 7 shows, for the bending test, the two mesh quality measures (defined based on the inner elements) plotted as functions of the bending magnitude for the standard technique, SEMMT-SD, and SEMMT-MD. Reductions in distortion over the standard technique of approximately 84–91% are experienced for the SEMMT-SD approach. The reductions are approximately 88–93% for the SEMMT-MD approach.

4. 2D fluid–structure interaction model problem

Test computations were carried out for a simple, 2D fluid–structure interaction (FSI) model problem to assess the effectiveness of the SEMMT for problems involving arbitrary deformations. The 2D model

represents a parachute-like structure. The "canopy" is modeled with 50 membrane elements and the "suspension lines" with 22 cable elements. In the initial, unstressed configuration the canopy section is a half-circle with a diameter (d) of 1.0 m and a depth of 0.04 m. The membrane has a thickness of 0.0002 m, a Poisson's ratio of 0.3, and a Young's modulus of 2.5×10^6 N/m^2. The total mass of the canopy is 0.0063 kg. For the suspension lines, the initial length is 0.90 m, the cross-sectional areas is 0.0002 m^2, and the Young's modulus is 5.0×10^6 N/m^2.

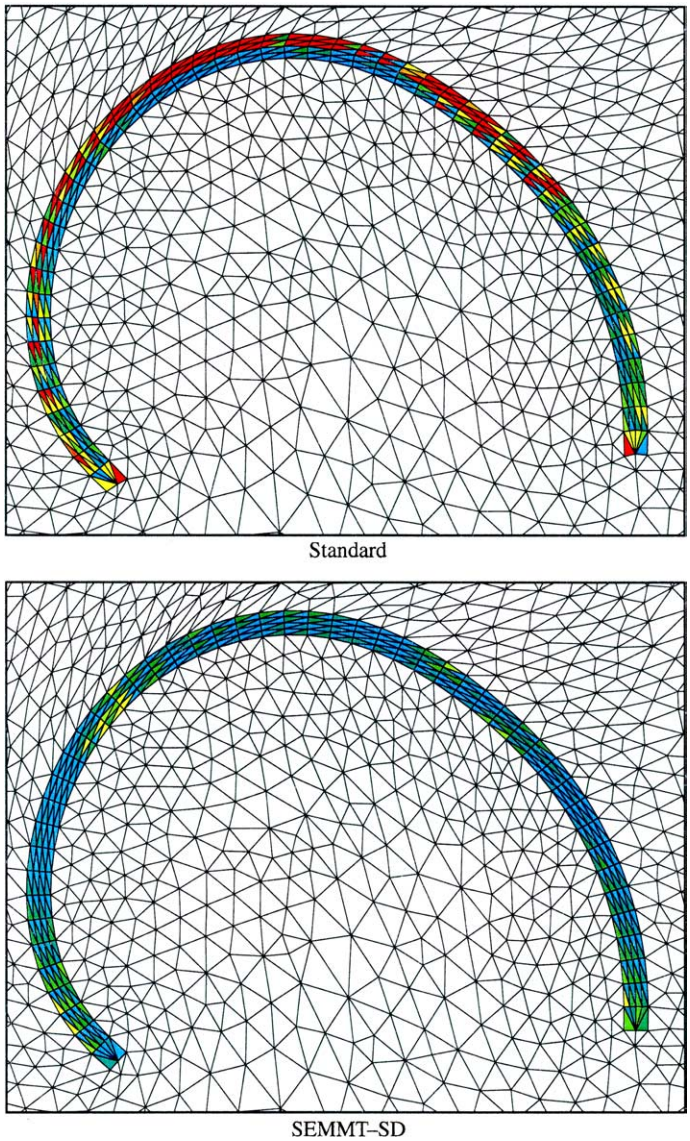

Fig. 8. Mesh deformations of the FSI model problem for the standard mesh moving technique and SEMMT-SD. Colors of the inner elements indicate element deformations as measured by the area change. The color range from light blue to light red corresponds to the range $0 \leqslant f_A^e \leqslant 0.04$.

First the "parachute" is inflated by carrying out a stand-alone structural dynamics computation with a prescribed canopy differential pressure of 0.5 N/m^2. A mass-proportional damping is employed in this computation to obtain a stable equilibrium for the inflated parachute. Then the fluid dynamics mesh is generated with the inflated canopy as an interior surface. Two layers of elements extend outward from the upper and lower surfaces of the canopy. The initial flow conditions for the FSI simulation are obtained by carrying out a stand-alone fluid dynamics computation with the canopy held rigid. For this computation, as well the subsequent FSI computation, a free-stream velocity of 0.35 m/s is prescribed at the inflow boundary, the fluid density is 1.0 kg/m^3, and the Reynolds number is 1000. The FSI computation is carried out for 500 time steps, with no structural damping. In 500 time steps fluid particles at free-stream velocity travel a distance of $1.75d$.

The deformed meshes in the vicinity of the canopy are shown for the standard mesh moving technique and SEMMT-SD in Figs. 8 and 9. In this test computation, the element distortions as measured by the aspect ratio change are more severe than the element deformations as measured by the area change. We can clearly see that the orthogonality of the mesh lines at the canopy surface is much better preserved with the SEMMT-SD. Fig. 10 shows the time evolution of the two mesh quality measures (defined based on the inner elements) during the FSI computations with the standard mesh moving technique and SEMMT-SD. In addition to the two measures based on the $p = \infty$ norm, we show the two measures based on the $p = 2$ norm to depict the mesh distortion for the inner elements in an averaged sense. From all four measures we can clearly see that, compared to the standard mesh moving technique, the SEMMT-SD yields significant reductions in distortion of the inner elements.

5. Concluding remarks

We have presented the SEMMT, which was introduced for the purpose of limiting mesh distortion in the layers of thin elements near fluid–structure interfaces. The SEMMT is built upon a class of mesh moving techniques where the motion of the nodes is governed by the equations of elasticity. In this class of techniques, deformation of the elements are treated selectively based on element sizes as well as deformation modes in terms of shape and volume changes. Smaller elements, typically placed near solid surfaces, are stiffened more than the larger ones. This is attained by altering the way we account for the Jacobian of the transformation from the element domain to the physical domain. The degree by which the smaller elements are stiffened more than the larger ones is determined by a stiffening power introduced into the formulation. Selection of optimal stiffening power allows for significant improvement in mesh quality near the solid surfaces, even when the displacements are large. In the SEMMT the layers of thin fluid elements are treated much like an extension of the solid elements.

The 2D tests presented here demonstrate how the SEMMT functions as part of our mesh update method. We employed two options of the SEMMT. In SEMMT-MD, the elasticity equations for the nodes connected to the thin (inner) elements are solved separately from the elasticity equations for the outer nodes. For the inner elements, as boundary conditions at the interface with the outer elements, we use traction-free conditions. In SEMMT-SD, the elasticity equations for the inner and outer nodes are solved together, but we assign higher rigidity to the inner elements. The test computations for translation, rotation, and bending tests show that the SEMMT results in significant improvements in mesh quality for the inner elements, with reductions in mesh distortion of 92–100% for prescribed translations, 91–98% for prescribed rotations, and 84–93% for prescribed bending. Additionally, the SEMMT yields similar improvements in computation of a simple, 2D fluid–structure interaction model problem with arbitrary deformations. These examples indicate that SEMMT can effectively handle mesh moving in thin layers of elements and is well-suited for certain classes of problems involving fluid–structure interactions.

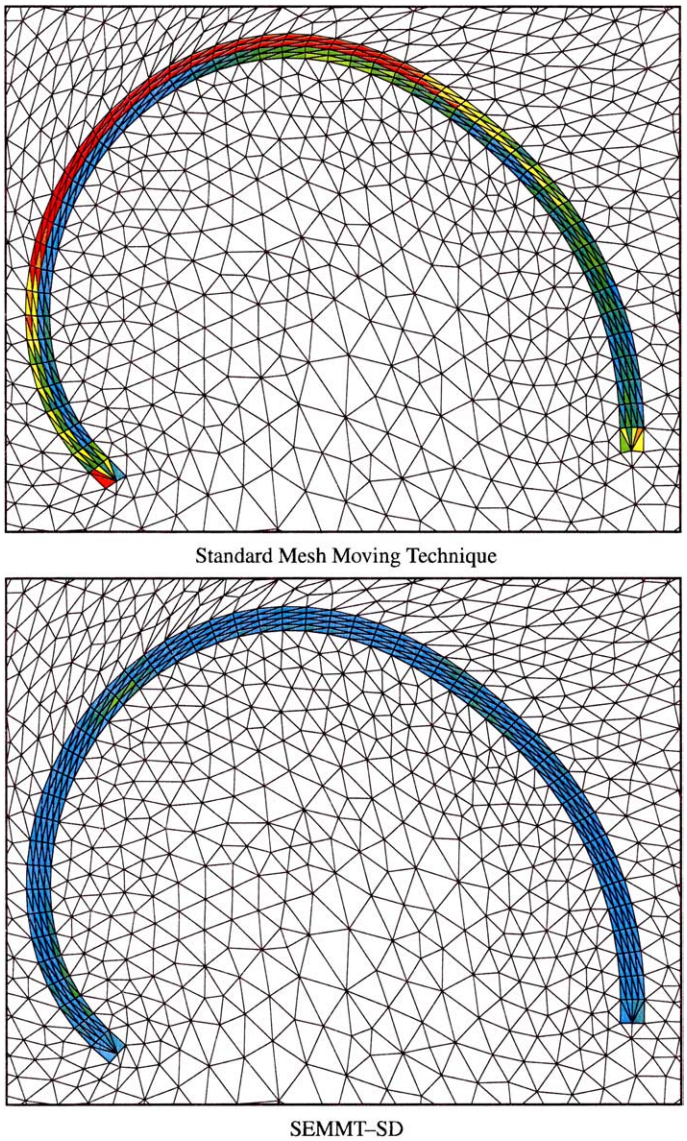

Fig. 9. Mesh deformations of the FSI model problem for the standard mesh moving technique and SEMMT-SD. Colors of the inner elements indicate element distortions as measured by the aspect ratio change. The color range from light blue to light red corresponds to the range $0 \leqslant f^e_{AR} \leqslant 0.25$.

Furthermore, we expect that the SEMMT will allow us explore new ways addressing contact problems that might be encountered in fluid–structure interactions.

Acknowledgements

This work was supported by the Army Natick Soldier Center and NASA JSC.

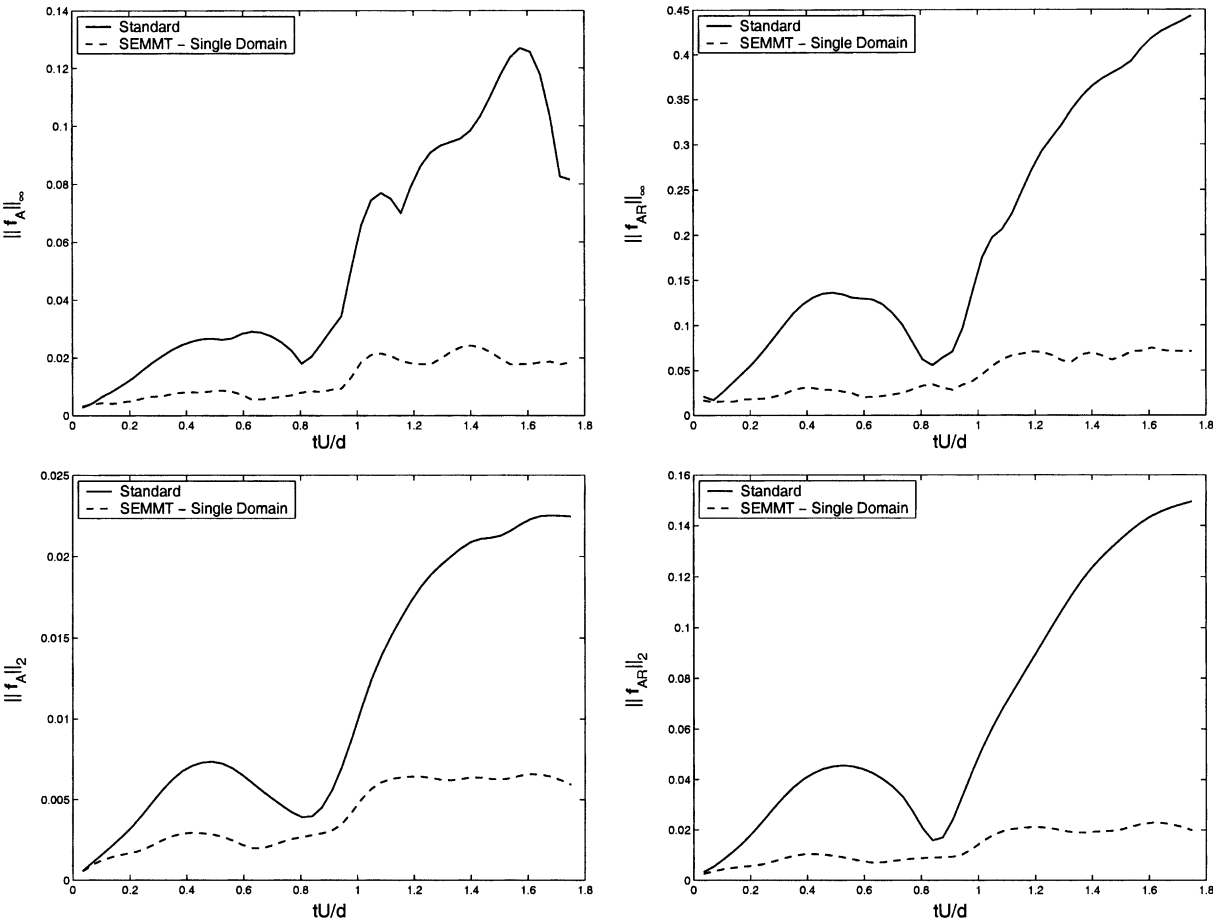

Fig. 10. Time evolution of the mesh quality measures (defined based on the inner elements) during the FSI computations with the standard mesh moving technique and SEMMT-SD.

References

[1] T.E. Tezduyar, Stabilized finite element formulations for incompressible flow computations, Adv. Appl. Mech. 28 (1991) 1–44.

[2] T.E. Tezduyar, M. Behr, J. Liou, A new strategy for finite element computations involving moving boundaries and interfaces—the deforming-spatial-domain/space–time procedure: I. The concept and the preliminary tests, Comput. Methods Appl. Mech. Engrg. 94 (3) (1992) 339–351.

[3] T.E. Tezduyar, M. Behr, S. Mittal, J. Liou, A new strategy for finite element computations involving moving boundaries and interfaces—the deforming-spatial-domain/space–time procedure: II. Computation of free-surface flows, two-liquid flows, and flows with drifting cylinders, Comput. Methods Appl. Mech. Engrg. 94 (3) (1992) 353–371.

[4] T.E. Tezduyar, M. Behr, S. Mittal, A.A. Johnson, Computation of unsteady incompressible flows with the finite element methods—space–time formulations, iterative strategies and massively parallel implementations, in: New Methods in Transient Analysis, PVP-vol. 246/AMD-vol. 143, ASME, New York, 1992, pp. 7–24.

[5] A. Masud, T.J.R. Hughes, A space–time Galerkin/least-squares finite element formulation of the Navier–Stokes equations for moving domain problems, Comput. Methods Appl. Mech. Engrg. 146 (1997) 91–126.

[6] K. Stein, T. Tezduyar, R. Benney, Mesh moving techniques for fluid–structure interactions with large displacements, J. Appl. Mech. 70 (2003) 58–63.

[7] T. Tezduyar, S. Aliabadi, M. Behr, A. Johnson, S. Mittal, Parallel finite-element computation of 3D flows, IEEE Comput. 26 (10) (1993) 27–36.

[8] T. Tezduyar, Finite element interface-tracking and interface-capturing techniques for flows with moving boundaries and interfaces, in: Proceedings of the ASME Symposium on Fluid-Physics and Heat Transfer for Macro- and Micro-Scale Gas–Liquid and Phase-Change Flows (CD-ROM), ASME Paper IMECE2001/HTD-24206, ASME, New York, 2001.
[9] T.E. Tezduyar, Stabilized finite element formulations and interface-tracking and interface-capturing techniques for incompressible flows, in: M. Hafez (Ed.), Numerical Simulations of Incompressible Flows, World Scientific, New Jersey, 2003, pp. 221–239.
[10] K. Stein, T. Tezduyar, Advanced mesh update techniques for problems involving large displacements, in: Proceedings of the Fifth World Congress on Computational Mechanics, On-line publication: http://wccm.tuwien.ac.at/, Paper-ID: 81489, Vienna, Austria, 2002.
[11] A.A. Johnson, T.E. Tezduyar, Simulation of multiple spheres falling in a liquid-filled tube, Comput. Methods Appl. Mech. Engrg. 134 (1996) 351–373.